

Non-equilibrium dynamics of ultracold lattice bosons inside a cavity

Huan Wang,^{1,*} Xiayao He,^{1,*} Shuai Li,¹ Hongrong Li,¹ and Bo Liu^{1,†}

¹*MOE Key Laboratory for Nonequilibrium Synthesis and Modulation of Condensed Matter, Shaanxi Province Key Laboratory of Quantum Information and Quantum Optoelectronic Devices, School of Physics, Xi'an Jiaotong University, Xi'an 710049, China*

We study the non-equilibrium quench dynamics crossing a continuous phase transition between the charge density wave (CDW) and supersolid (SS) phases of a bosonic lattice gas with cavity-mediated interactions. When changing the hopping amplitude in the Hamiltonian as a function of time, we investigate the scaling behavior of the correlation length and vortex density with respect to the quench time and find that there is a threshold of the quench rate separating two distinct scaling regimes. When slowly varying the system below that threshold, we find a power-law scaling as predicted by the Kibble-Zurek mechanism (KZM). While considering fast quench above that threshold, a deviation from the KZM prediction occurs, manifested by a saturation of the defect density. We further show that such distinct scaling behaviors during different dynamic procedures can be understood through comparing the relaxation time and the quench rate.

I. INTRODUCTION

The study of dynamics of quantum many-body system is one of the most exciting frontiers in modern condensed matter physics [1, 2]. The so-called Kibble-Zurek mechanism (KZM) has been used to understand certain universal features of the dynamics across a continuous phase transition both in classical [3–7] and quantum [1, 2, 8–15] realms. Based on conventional scaling laws near the criticality, KZM predicts a universal scaling for resulting density of defects when the system crosses a second-order phase transition by a linear quench. Recently, tremendous amount of efforts in both theoretical and experimental studies have been triggered to explore such quench dynamics, for instance in liquid crystals [16, 17], quantum optical systems [18], superconducting films [19, 20], trapped ions [21–26], as well as ultracold gases [27–32].

In particular, ultracold gases in optical lattices provide a versatile tool for simulating and studying dynamics of quantum many-body physics [33–37], including the early studies of single-component bosonic lattice gases [30–32], Rydberg-dressed atoms [38, 39] and dipolar bosons [40] in optical lattices. Lots of interesting properties of these systems, such as verifying the Kibble-Zurek (KZ) scaling law between the defect formation and quench rate [28, 29, 41, 42], have already been well studied. At the same time, there has also been a great interest in exploring the deviation from the KZ scaling in quench dynamics across the critical regime of the phase transition. Various new effects, such as new statistics of the resulting defects [43, 44], fantastic evolution of correlation functions [45] and unusual saturation of the defect density [46–51] have been unveiled.

In this work, motivated by recent progresses in experimental investigation of the bosonic lattice gas inside a cavity [52, 53], where the effect of cavity-mediated in-

teractions result in the observation of a rich equilibrium phase diagram including Mott insulator (MI), superfluid (SF), supersolid (SS) and charge-density-wave (CDW) phases, we study its non-equilibrium quench dynamics. This set-up offers new possibilities for exploring various non-equilibrium dynamics via varying the parameters of the Hamiltonian crossing different quantum phase transitions (QPT). And here we focus on studying the quench dynamics across the continuous phase transition between the CDW and SS phases. It is found that there is a threshold of the quench rate. Below that threshold, various physical quantities, such as the correlation length and vortex density, show a good agreement with the KZ scaling law. While above that threshold, the saturation of the defect density has been found, indicating a deviation of the KZ scaling at fast quench.

This paper is organized as follows. In Section II, through employing the static Gutzwiller (GW) method, the equilibrium phase diagram is obtained, which is consistent with other mean-field calculations. In Section III, the protocol of quench is introduced and the non-equilibrium quench dynamics across the continuous phase transition between the CDW and SS phases have been studied by the time-dependent Gutzwiller (tGW) method. The scaling laws of the correlation length and the number of defects have been investigated. It is shown that there is a threshold of the quench rate separating two distinct scaling regimes. One is satisfied with the KZ scaling law, the other is characterized with the saturation of defect density, showing a deviation from the KZ scaling. We further show that such distinct scaling behaviors can be understood through comparing the relaxation time and the quench rate.

II. EFFECTIVE MODEL AND EQUILIBRIUM PHASE DIAGRAM

Let us consider load a Bose-Einstein condensate (BEC) of ⁸⁷Rb into a highly anisotropic 3D optical lattice coupled to an ultrahigh-finesse optical cavity, being simi-

* These authors contribute equally to this work.

† liubophy@gmail.com

lar as the ETH experimental setup [52]. Since the coherent scattering of light between the lattice and cavity modes creates a dynamical checkerboard superlattice for the atoms [54–56], the effective Hamiltonian describing the atomic dynamics dressed by the cavity field can be expressed as

$$H = -J \sum_{\langle i,j \rangle} (\hat{b}_i^\dagger \hat{b}_j + h.c.) + \frac{U}{2} \sum_{i \in e,o} \hat{n}_i (\hat{n}_i - 1) - \frac{U_L}{N} \left(\sum_{i \in e} \hat{n}_i - \sum_{i \in o} \hat{n}_i \right)^2 - \mu \sum_{i \in e,o} \hat{n}_i, \quad (1)$$

where \hat{b}_i and \hat{b}_i^\dagger are the annihilation and creation operators for bosonic atoms at the lattice site \mathbf{r}_i . e and o refer to the even and odd sites of the lattice, respectively. $\hat{n}_i = \hat{b}_i^\dagger \hat{b}_i$ is the on-site particle number operator. N is the total number of lattice sites. J captures the tunneling amplitude between nearest neighbors and μ is the chemical potential. The strength of the on-site repulsion is labeled as U , which can be tuned through the Feshbach resonance technics. $U_L = -N\hbar M_0^2 \eta^2 / \Delta_c$ describes the strength of the cavity-mediated interaction between atoms, where M_0 is the overlap between the Wannier function and the lattice potential ($\propto \cos \frac{2\pi x}{\lambda} \cos \frac{2\pi y}{\lambda}$) and η is the two-photon Rabi frequency of the scattering process. $\Delta_c = \omega_p - \omega_c$ represents the dispersive shift of pumping frequency ω_p and cavity resonance frequency ω_c .

The cavity-mediated interaction (U_L term in Eq. (1)) favors an overall even-odd sites imbalance, which can be characterized by the defined charge-density-wave (CDW) order parameter as $\theta = 2 \langle (\sum_{i \in e} \hat{n}_i - \sum_{i \in o} \hat{n}_i) \rangle / N$, where $\langle \dots \rangle$ means the expectation value in the ground state. The superfluid order parameters for the even and odd lattice sites are introduced as $\phi_{e/o} = \langle b_{e/o} \rangle$, respectively. Then, we employ the static Gutzwiller (GW) method to study the equilibrium zero-temperature phase diagram of the system. Consider starting with the GW ansatz

$$|\Psi_{gw}\rangle = \prod_i \sum_{n_i=0}^{n_{max}} f_{n_i}^{(i)} |n_i\rangle, \quad (2)$$

where $i \in e, o$ and $f_{n_e}^{(e)}$, $f_{n_o}^{(o)}$ are the variational coefficients. n_{max} is the maximum number of particles at each site. Then, the above defined order parameters can be rewritten as

$$\phi_i = \sum_{n_i=0}^{n_{max}-1} \sqrt{n_i+1} f_{n_i}^{(i)*} f_{n_i+1}^{(i)},$$

$$\theta = \frac{2}{N} \left(\sum_{i \in e} \sum_{n_i=0}^{n_{max}} |f_{n_i}^{(i)}|^2 n_i - \sum_{i \in o} \sum_{n_i=0}^{n_{max}} |f_{n_i}^{(i)}|^2 n_i \right). \quad (3)$$

Here, we take $n_{max} = 7$ for both even and odd sites, which is proved to be large enough for the study of our proposed system. The average number density

of atoms is determined through the relation $\langle n_i \rangle = \sum_{n_i=0}^{n_{max}} |f_{n_i}^{(i)}|^2 n_i$. By minimizing the expectation ground state energy $\langle \Psi_{gw} | H | \Psi_{gw} \rangle$, the variational coefficients in $|\Psi_{gw}\rangle$ can be determined (see Appendix A for details). Therefore, order parameters defined above can be obtained through the GW method. The equilibrium zero-temperature phase diagram can thus be obtained, such as shown in Fig. 1(a). The difference among distinct phases can be captured by the order parameters, for example, as shown in Fig. 1(b). In the supersolid (SS) phase, a finite even-odd imbalance and nonzero superfluid order parameters coexist, which is distinct from a superfluid (SF) phase where the even-odd imbalance is vanished and there is finite and equal superfluid order parameters. In the charge-density-wave (CDW) state, superfluid order parameters vanish. And the presence of a finite even-odd imbalance distinguishes the CDW from a Mott insulator (MI) state. Our phase diagram is in good agreement with other existing studies [56–62].

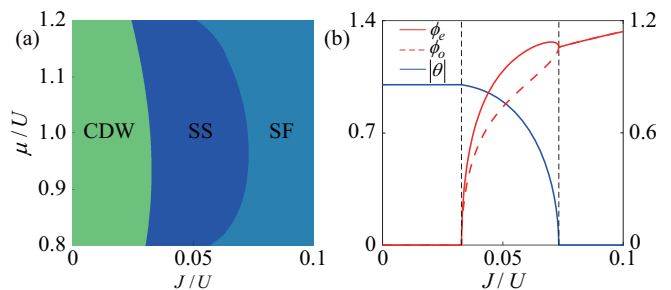


Fig. 1. (a) Equilibrium zero-temperature phase diagram as a function of the hopping amplitude and chemical potential with $U_L/U = 0.5$. (b) Superfluid order parameters $\phi_{e(o)}$ and the average imbalance θ between even and odd lattice sites as a function of hopping amplitude. Here we choose $\mu/U = 0.95$ and other parameters are the same as in (a).

III. QUENCH DYNAMICS ACROSS THE PHASE TRANSITION FROM CDW TO SS

In this section, we will study the dynamics across the phase transition from CDW to SS as shown in Fig. 1(a). The quench protocol is constructed through tuning the tunneling amplitude J by the following relation

$$J(t) = \begin{cases} J_i + \frac{J_f - J_i}{2\tau_Q} (t + \tau_Q) & t \in [-\tau_Q, \tau_Q] \\ J_f & t > \tau_Q \end{cases} \quad (4)$$

where J_i and J_f are the initial and final values of the quench tunneling amplitude, which satisfy the relations $J_i < J_{c1}$ and $J_{c1} < J_f < J_{c2}$ with J_{c1} and J_{c2} being the equilibrium phase transition points of CDW to SS and SS to SF as shown in Fig. 1(a), respectively. Here $J_f + J_i = 2J_{c1}$ means that the system approaches the quantum critical point between CDW and SS at $t = 0$.

τ_Q is the quench time, which captures the quench rate. We then employ the time-dependent Gutzwiller (tGW) method for investigating the real-time dynamics of our proposed system via varying $J(t)$ as in Eq.(4). In the practical calculation, we use the interaction strength U as the unit of energy and \hbar/U is used as the unit of time t . In the tGW approximation, the Hamiltonian in Eq. (1) is devised into a single-site Hamiltonian and can be approximated as H_{GW} (see details in Appendix B). Then, we introduce the tGW wave function as

$$|\Psi_{tgw}\rangle = \prod_i \sum_{n_i=0}^{n_{max}} f_{n_i}^{(i)}(t) |n_i\rangle. \quad (5)$$

The coefficients $f_{n_i}^{(i)}(t)$ can be determined by solving the following Schrödinger equation $i\hbar\partial_t |\Psi_{tgw}(t)\rangle = H_{GW}(t) |\Psi_{tgw}(t)\rangle$ for various initial states corresponding to the CDW phase and $H_{GW}(t)$ comes from replacing J by $J(t)$ in H_{GW} . Therefore, the coefficients of tGW wave function can be determined through the following relation

$$\begin{aligned} \frac{i\hbar\partial f_{n_i}^{(i)}(t)}{\partial t} = & -J(t) \sum_{\langle i,j \rangle} [\phi_j^* \sqrt{n_i+1} f_{n_i+1}^{(i)}(t) + \phi_j \sqrt{n_i} f_{n_i-1}^{(i)}(t)] \\ & + [\frac{U}{2} n_i(n_i-1) - \mu n_i] f_{n_i}^{(i)}(t) - (-1)^i \theta U_L n_i f_{n_i}^{(i)}(t) \end{aligned} \quad (6)$$

Then, we use the fourth-order Runge-Kutta method to study the time evolution of the system and calculate various physical quantities, such as the SF order parameter Φ , correlation length ξ and vortex number N_v , which are defined as follows

$$\begin{aligned} \Phi &= \frac{1}{N} \sum_i |\phi_i|, \\ \langle b_i^\dagger b_j \rangle &\propto \exp\left(-\frac{|\mathbf{r}_i - \mathbf{r}_j|}{\xi}\right), \\ N_v &= \sum_i |\Omega_i|, \end{aligned} \quad (7)$$

where $\Omega_i = \frac{1}{4}[\sin(\theta_{i+\hat{e}_x} - \theta_i) + \sin(\theta_{i+\hat{e}_x+\hat{e}_y} - \theta_{i+\hat{e}_x}) + \sin(\theta_{i+\hat{e}_y} - \theta_{i+\hat{e}_x+\hat{e}_y}) + \sin(\theta_i - \theta_{i+\hat{e}_y})]$ with θ_i being the phase of superfluid order parameter ϕ_i and $\hat{e}_x(\hat{e}_y)$ being the unit vector along the $x(y)$ direction. The system size is chosen as 100×100 in most of our numerical calculations and we have verified that this is a sufficiently large size where the size-dependent effect disappears.

As shown in Fig. 2, the typical behavior of SF order parameter Φ as the function of time t is demonstrated. At $t = 0$, the system crosses the quantum critical point between CDW and SS at J_{c1} and the relaxation time of the system diverges. The dynamics is thus frozen and the state of the system cannot follow the change in the hopping amplitude. This scenario persists till the transition time \hat{t} , which is determined by the relation $|\Phi(\hat{t})| = 2|\Phi(t=0)|$. Then, Φ develops very rapidly. After that rapid increase, Φ starts to fluctuate and such

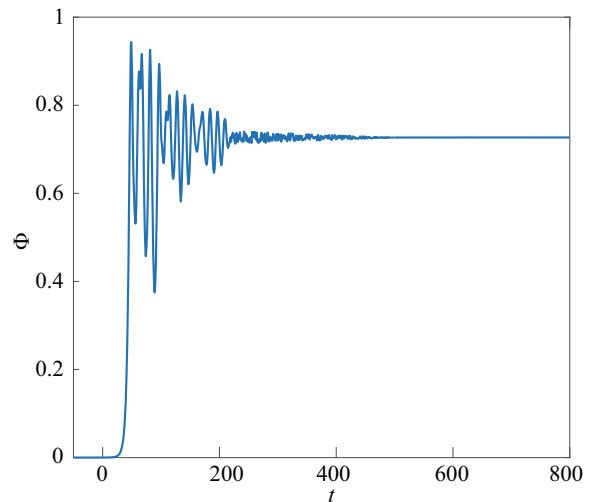


Fig. 2. Time evolution of the defined SF order parameter Φ . Here we consider changing the hopping amplitude from $J_i/U = 0$ to $J_f/U = 0.0658$ linearly during the time interval $2\tau_Q$ with $\tau_Q = 50$. Time is in the unit of \hbar/U and $\mu/U = 0.95$. At $t = 0$, the system passes through the equilibrium phase transition point from CDW to SS.

an oscillatory trend sets the average value tend towards the steady state value. We also study the defects formation during the course of the quench dynamics by investigating the vortex number N_v defined above, as an indicator of the defect density. When the quench dynamics in the CDW region, the vortex density is high, which is caused by the effect of phase fluctuations introduced during the initial state preparation. Then, at $t = 0$ the system crosses the quantum critical point and enters into the SS regime where spontaneous symmetry breaking occurs. The SF order parameters acquire finite values and small domains are gradually formed (shown in Fig. 3). However, such domains are formed where there is a phase coherence within, but not between the domains. As the quench is continued further, due to the annihilation of vortex-antivortex pairs, domains are merged and the size of domain becomes larger. The number of that thus decreases. After approaching the steady state, phase coherence is established in the system and the vortex number approaches zero.

Next, we will investigate the behavior of quench dynamics with different quench rate ($\propto 1/\tau_Q$). To study the scaling laws for the above defined quantities, such as correlation length ξ and vortex number N_v , with respect to the quench time, we monitor ξ and N_v at the transition time \hat{t} , because \hat{t} captures the freeze out time indicating the moment that the system catches the quench speed beginning to evolve quickly and can thus be linked to the universal scaling law connected with the relaxation time. As shown in Fig. 4, there are two different regimes separating distinct scaling behaviors for both ξ and N_v as a function of τ_Q . For slow quench, such as τ_Q from $\tau_Q = 10$ to $\tau_Q = 400$ (Fig. 4), it is shown that both ξ and N_v sat-

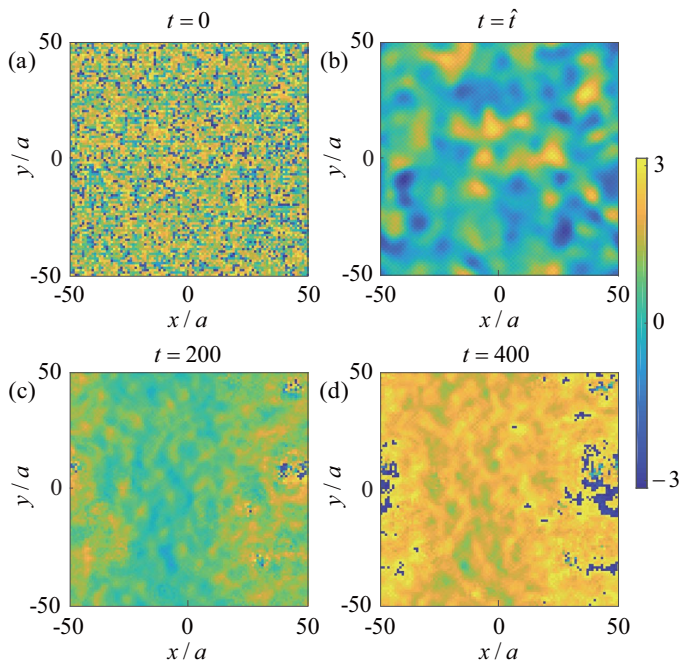


Fig. 3. Snapshots of the phase of the order parameter ϕ_i at certain times for $\tau_Q = 50$. As shown in (a), when $t = 0$, the system crosses the quantum critical point and enters into the SS regime, where the SF order parameters acquire finite values and small domains is gradually formed. As shown in (b)-(d), when the quench is continued further, domains are merged. The size of that becomes larger and the number of that thus decreases. a is the lattice constant. Other parameters are the same as in Fig. 2.

isfy a fairly good scaling law as $\xi \propto \tau_Q^b$ and $N_v \propto \tau_Q^{-d}$ with $b \approx 0.33$ and $d \approx 0.64$, respectively. The relation $d \approx 2b$ holds. Therefore, the KZ hypothesis predicted power law scaling is satisfied in the slow quench regime. Moreover, the KZM also predicts that the transition time \hat{t} should have the scaling law as $\hat{t} \sim \tau_Q^{\nu z / (1 + \nu z)}$ with ν and z being the critical exponent of the equilibrium correlation length and the dynamical critical exponent, respectively. Through extracting the exponent from the scaling of \hat{t} , such as shown in Fig. 4(c) and utilizing the relation $b = \frac{\nu}{1 + \nu z}$ and $d = \frac{2\nu}{1 + \nu z}$, ν and z can be estimated. We get $z \approx 0.98$ and $\nu \approx 0.49$, where z is fairly close to that expected value $z = 1$ from the 3D XY model, but ν dose not coincide with $\nu = 0.672$ predicated in the 3D XY model [63], indicating that the spatial inhomogeneity effects the critical behavior [32]. While considering fast quench, as shown in Fig. 4, it is found that the vortex defect density demonstrates a plateau whose value is a constant independent of the quench rate and $\xi(\hat{t})$ also has the similar behavior. It indicates that there is a violation of the KZ scaling in the fast quench regime.

In the following, we will make a detailed analysis of the above distinct scaling behaviors and determine the critical quench rate ($\propto 1/\tau_{Qc}$) separating two different quench regimes. To understand the quench dynamics

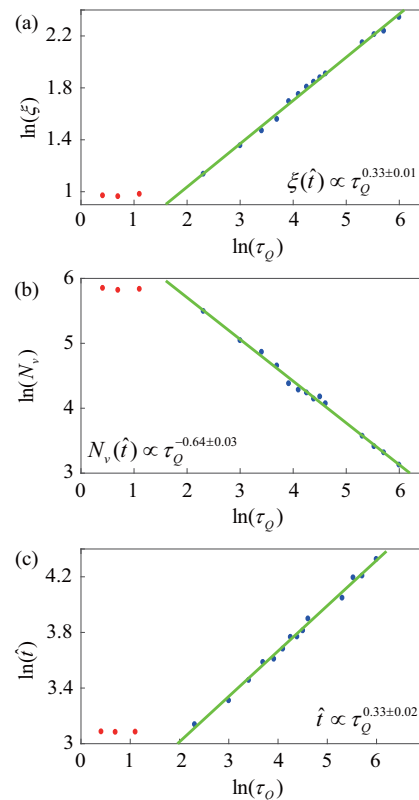


Fig. 4. (a) and (b): Scaling law of the correlation length ξ and vortex number N_v at $t = \hat{t}$ with respect to τ_Q . There are two distinct scaling regimes. One is in good agreement with the KZ scaling law, the other is characterized with the saturation of various quantities, indicating a deviation from the KZ scaling. (c) Scaling law of transition time $t = \hat{t}$ with respect to τ_Q . It has the similar behavior as (a) and (b). Other parameters are the same as in Fig. 2.

here, we first study the relaxation time of the system. Since the transition time \hat{t} captures the moment that the system catches the quench speed and begin to evolve quickly, it can be linked to the relaxation time τ through the following relation

$$\hat{t} = \tau(J(\hat{t})). \quad (8)$$

Therefore, through solving the above equation, the relaxation time can be obtained. As shown in Fig. 5, we display the relaxation time as a function of the hopping amplitude J . Through comparing the relaxation time and the quench rate, distinct scaling behaviors during the dynamic procedure can be understood. Let us consider fixing J_f at a certain value at $J_f = \bar{J}$. Then, various quench procedures with different quench time τ_Q can be distinguished by a critical quench time τ_{Qc} determined by the relation $J(\hat{t}) = \bar{J}$, for instance, as indicated by the blue-dashed line in Fig. 5. Therefore, τ_{Qc} can be determined by the slope of that blue-dashed line decides a threshold of the quench rate separating two distinct scaling regime. Let us first consider the fast quench above that threshold. For example, as indicated by the red-

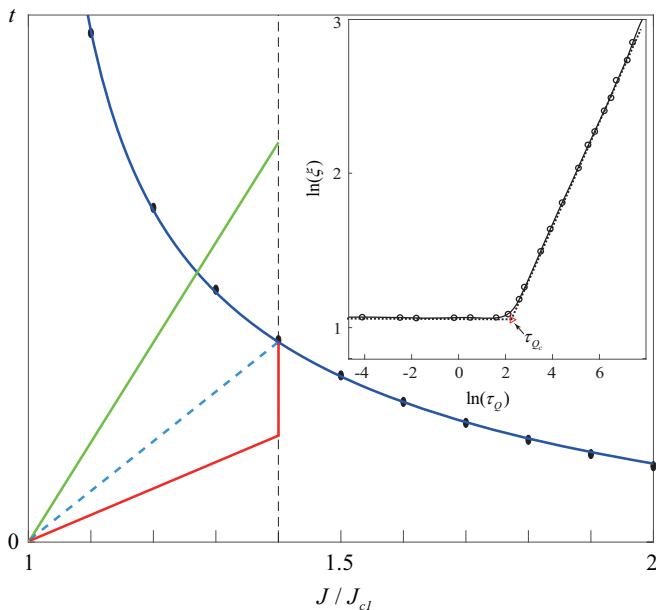


Fig. 5. The relaxation time as a function of hopping amplitude (blue-solid line). The slope of blue-dashed line decides the threshold of quench rate separating two distinct scaling regime when fixing $J_f = \bar{J}$ with $\bar{J}/J_{c1} = 1.4$. The red-solid line indicates one of the fast quench above the threshold, where a deviation from the KZM predicted scaling occurs. The green-solid line stands for one of the slow quench below the threshold, where the adiabatic-impulse approximation is valid and the KZ scaling thus be satisfied. The inset shows that the intersection point of the un-smooth transition from the plateau to KZM power law scaling of the correlation length can also determine the critical quench time τ_{Qc} .

solid line in Fig. 5, the linear quench ends before the time that such line (stands for $J(t)$) meets the $\tau(J)$ line. Therefore, the transition time \hat{t} for any fast quench above the threshold of the quench rate will be the same and be fixed at $\hat{t} = \tau(\bar{J})$, being independent of the values of τ_Q . The domains of defect for different quench rates will thus have the same average size, which naturally explains the plateau of defect density appears in rapidly quenched dynamics. While considering the slow quench below that threshold, for instance, as indicated by the green-solid line in Fig. 5, the $J(t)$ line intersects the $\tau(J)$ line before the end of linear quench. It means that the system cannot follow the change of $J(t)$ and the dynamics is frozen, which will persist till the transition time marking the impulse period of the quench. After the evolution time is equal to the relaxation time, the system evolves promptly. Therefore, the adiabatic-impulse approximation is valid and the KZ scaling is satisfied. Furthermore,

the critical quench time τ_{Qc} can also be determined by the intersection point of the un-smooth transition from the plateau to KZM power law scaling of the correlation length or vortex density, for instance as shown by the dashed-line in the inset of Fig. 5. The obtained critical quench time τ_{Qc} is consistent with the way through comparing the relaxation time and the quench rate as mentioned above.

IV. CONCLUSION

In conclusion, we have examined the quench dynamics crossing a continuous phase transition between CDW and SS phases of a bosonic lattice gas with cavity-mediated interactions. By using the time-dependent Gutzwiller method, we find that various physical quantities, such as the correlation length and vortex density, show two distinct scaling regimes with respect to the quench time. There is a threshold of quench rate. Below that, the scaling behavior is in good agreement with the KZ scaling law. When above that threshold, the scaling behavior is characterized with the saturation of various quantities, indicating a deviation from the KZ scaling. Furthermore, our proposal can be viably simulated experimentally in ultracold gases, since such a system has already been implemented in experiments. It thus paves an alternative way for investigating the dynamics of the system combined with the cavity light and interacting quantum matters.

ACKNOWLEDGMENTS

This work is supported by the National Key R&D Program of China (2021YFA1401700), NSFC (Grant No. 12074305, 12147137, 11774282, 11950410491), the National Key Research and Development Program of China (2018YFA0307600), the Fundamental Research Funds for the Central Universities and Cyrus Tang Foundation Young Scholar Program (H. W., X. H., S. L. and B. L.). We also thank M. Arzamasovs for helpful discussions and the HPC platform of Xi'an Jiaotong University, where our numerical calculations was performed.

Appendix A: Static Gutzwiller Method

To employ the static Gutzwiller method for studying the equilibrium zero-temperature phase diagram of the system, we apply the GW ansatz $|\Psi_{gw}\rangle$ to the model Hamiltonian in Eq. (1). Then, the expectation value for each terms in the Hamiltonian can be expressed in terms of $f_{n_i}^{(i)}$ by using the following relations

$$\begin{aligned}
\langle b_i^\dagger b_j \rangle &= \left(\sum_{n_i=0}^{n_{\max}-1} f_{n_i+1}^{(i)*} f_{n_i}^{(i)} \sqrt{n_i+1} \right) \left(\sum_{n_j=0}^{n_{\max}-1} f_{n_j}^{(j)*} f_{n_j+1}^{(j)} \sqrt{n_j+1} \right) \\
\langle b_i^\dagger b_i \rangle &= \sum_{n_i=0}^{n_{\max}} \left| f_{n_i}^{(i)} \right|^2 n_i \\
\langle b_i \rangle &= \sum_{n_i=0}^{n_{\max}-1} f_{n_i}^{(i)*} f_{n_i+1}^{(i)} \sqrt{n_i+1}
\end{aligned} \tag{A1}$$

The expectation ground state energy $\langle \Psi_{gw} | H | \Psi_{gw} \rangle$ can

thus be obtained as

$$\begin{aligned}
\langle H \rangle &= -J \sum_{\langle i,j \rangle} \left[\left(\sum_{n_i=0}^{n_{\max}-1} f_{n_i+1}^{(i)*} f_{n_i}^{(i)} \sqrt{n_i+1} \right) \left(\sum_{n_j=0}^{n_{\max}-1} f_{n_j}^{(j)*} f_{n_j+1}^{(j)} \sqrt{n_j+1} \right) + \left(\sum_{n_j=0}^{n_{\max}-1} f_{n_j+1}^{(j)*} f_{n_j}^{(j)} \sqrt{n_j+1} \right) \left(\sum_{n_i=0}^{n_{\max}-1} f_{n_i}^{(i)*} f_{n_i+1}^{(i)} \sqrt{n_i+1} \right) \right] \\
&\quad - \frac{U_L}{N} \left[\left(\sum_{i \in e} \sum_{n_i=0}^{n_{\max}} \left| f_{n_i}^{(i)} \right|^2 n_i \right)^2 + \left(\sum_{i \in o} \sum_{n_i=0}^{n_{\max}} \left| f_{n_i}^{(i)} \right|^2 n_i \right)^2 - 2 \left(\sum_{i \in e} \sum_{n_i=0}^{n_{\max}} \left| f_{n_i}^{(i)} \right|^2 n_i \right) \left(\sum_{i \in o} \sum_{n_i=0}^{n_{\max}} \left| f_{n_i}^{(i)} \right|^2 n_i \right) \right] \\
&\quad + \frac{U}{2} \sum_i \sum_{n_i=0}^{n_{\max}} \left| f_{n_i}^{(i)} \right|^2 n_i (n_i - 1) - \mu \sum_i \sum_{n_i=0}^{n_{\max}} \left| f_{n_i}^{(i)} \right|^2 n_i
\end{aligned} \tag{A2}$$

By minimizing $\langle \Psi_{gw} | H | \Psi_{gw} \rangle$ with respect to a set of amplitudes $f_{n_i}^{(i)}$, we can determine the ground state of the system. Different order parameters defined in Eq. (3) can thus be calculated via $f_{n_i}^{(i)}$. The equilibrium zero-temperature phase diagram can thus be obtained as shown in Fig. 1(a).

Appendix B: Time-dependent Gutzwiller method

To study quench dynamics of the system, we employ the time-dependent Gutzwiller (tGW) methods. The tGW methods approximate the Hamiltonian in Eq. (1) with a single-site Hamiltonian. To do that, we first treat with the cavity-mediated interaction term by the mean-field approximation as $-\frac{U_L}{N} \left(\sum_{i \in e} \hat{n}_i - \sum_{i \in o} \hat{n}_i \right)^2 \approx \frac{U_L N \theta^2}{4} -$

$U_L \theta \left(\sum_{i \in e} \hat{n}_i - \sum_{i \in o} \hat{n}_i \right)$, where θ describes imbalance between even and odd lattice sites as defined in Eq. (3). Then, the Hamiltonian in Eq. (1) can be approximated as

$$\begin{aligned}
H_{GW} &= \sum_i H_i \\
H_i &= -J \sum_{j \in iNN} \left(\hat{b}_i^\dagger \phi_j + H.c. \right) + \frac{U}{2} \hat{n}_i (\hat{n}_i - 1) - \mu \hat{n}_i \\
&\quad - (-1)^i U_L \theta \hat{n}_i,
\end{aligned} \tag{B1}$$

where iNN denotes the nearest-neighbor (NN) sites of i . The dynamics of the system can be determined by solving the following Schrödinger equation $i\hbar \partial_t |\Psi_{tgw}(t)\rangle = H_{GW}(t) |\Psi_{tgw}(t)\rangle$ via replacing J by $J(t)$ in H_{GW} .

-
- [1] A. Polkovnikov, K. Sengupta, A. Silva, and M. Vengalattore, *Rev. Mod. Phys.* **83**, 863 (2011).
 - [2] H. Aoki, N. Tsuji, M. Eckstein, M. Kollar, T. Oka, and P. Werner, *Rev. Mod. Phys.* **86**, 779 (2014).
 - [3] T. W. B. Kibble, *J. Phys. A* **9**, 1387 (1976).
 - [4] T. W. B. Kibble, *Phys. Rep.* **67**, 183 (1980).
 - [5] W. Zurek, *Nature (London)* **317**, 505 (1985).
 - [6] W. Zurek, *Acta Phys. Pol. B* **24**, 1301 (1993).
 - [7] W. Zurek, *Phys. Rep.* **276**, 177 (1996).
 - [8] B. Damski, *Phys. Rev. Lett.* **95**, 035701 (2005).
 - [9] W. Zurek, U. Dorner, and P. Zoller, *Phys. Rev. Lett.* **95**, 105701 (2005).
 - [10] A. Polkovnikov, *Phys. Rev. B* **72**, 161201(R) (2005).
 - [11] J. Dziarmaga, *Phys. Rev. Lett.* **95**, 245701 (2005).
 - [12] V. Mukherjee, U. Divakaran, A. Dutta, and D. Sen, *Phys. Rev. B* **76**, 174303 (2007).
 - [13] D. Sen, K. Sengupta, and S. Mondal, *Phys. Rev. Lett.* **101**, 016806 (2008).
 - [14] J. Dziarmaga, *Adv. Phys.* **59**, 1063 (2010).
 - [15] L. Cincio, J. Dziarmaga, J. Meisner, and M. M. Rams, *Phys. Rev. B* **79**, 094421 (2009).

- [16] M. J. Bowick, L. Chandar, E. A. Schiff, and A. M. Srivastava, *Science* **263**, 943 (1994).
- [17] S. Digal, R. Ray, and A. M. Srivastava, *Phys. Rev. Lett.* **83**, 5030 (1999).
- [18] X.-Y. Xu, Y.-J. Han, K. Sun, J.-S. Xu, J.-S. Tang, C.-F. Li, and G.-C. Guo, *Phys. Rev. Lett.* **112**, 035701 (2014).
- [19] A. Maniv, E. Polturak, and G. Koren, *Phys. Rev. Lett.* **91**, 197001 (2003).
- [20] D. Golubchik, E. Polturak, and G. Koren, *Phys. Rev. Lett.* **104**, 247002 (2010).
- [21] A. Chandran, A. Erez, S. Gubser, and S. Sondhi, *Phys. Rev. B* **86**, 064304 (2012).
- [22] A. Francuz, J. Dziarmaga, B. Gardas, and W. Zurek, *Phys. Rev. B* **93**, 075134 (2016).
- [23] A. Bermudez, D. Patane, L. Amico, and M. Martin-Delgado, *Phys. Rev. Lett.* **102**, 135702 (2009).
- [24] A. Bermudez, L. Amico, and M. Martin-Delgado, *New. J. Phys.* **12**, 055014 (2010).
- [25] J. Dziarmaga and W. Zurek, *Sci. Rep.* **4**, 5950 (2014).
- [26] B. Gardas, J. Dziarmaga, and W. Zurek, *Phys. Rev. B* **95**, 104306 (2017).
- [27] N. Navon, A. Gaunt, R. Smith, and Z. Hadzibabic, *Science* **347**, 167 (2015).
- [28] D. Chen, M. White, C. Borries, and B. DeMarco, *Phys. Rev. Lett.* **106**, 235304 (2011).
- [29] S. Braun, M. Friesdorf, S. S. Hodgman, M. Schreiber, J. P. Ronzheimer, A. Riera, M. del Rey, I. Bloch, J. Eisert, and U. Schneider, *Proc. Natl. Acad. Sci.* **112**, 3641 (2015).
- [30] K. Shimizu, Y. Kuno, T. Hirano, and I. Ichinose, *Phys. Rev. A* **97**, 033626 (2018).
- [31] K. Shimizu, T. Hirano, J. Park, Y. Kuno, and I. Ichinose, *New. J. Phys.* **20**, 083006 (2018).
- [32] K. Shimizu, T. Hirano, J. Park, Y. Kuno, and I. Ichinose, *Phys. Rev. A* **98**, 063603 (2018).
- [33] D. Jaksch, C. Bruder, J. Cirac, C. Gardiner, and P. Zoller, *Phys. Rev. Lett.* **81**, 3108 (1998).
- [34] M. Greiner, O. Mandel, T. Esslinger, T. Hansch, and I. Bloch, *Nature* **415**, 39 (2002).
- [35] I. Bloch, J. Dalibard, and W. Zwerger, *Rev. Mod. Phys.* **80**, 885 (2008).
- [36] J. Cirac and P. Zoller, *Nat. Phys.* **8**, 264 (2012).
- [37] *Ultracold Atoms in Optical Lattices: Simulating Quantum Many-body Systems* (OUP, 2012).
- [38] Y. Zhou, Y. Li, R. Nath, and W. Li, *Phys. Rev. A* **101**, 013427 (2020).
- [39] A. Keesling, A. Omran, H. Levine, H. Bernien, H. Pichler, S. Choi, R. Samajdar, S. Schwartz, P. Silvi, S. Sachdev, et al., *Nature* **568**, 207 (2019).
- [40] H. Sable, D. Gaur, S. Bandyopadhyay, R. Nath, and D. Angom, arXiv:2106.01725 (2021).
- [41] M. Anguez, B. A. Robbins, H. M. Bharath, M. Boguslawski, T. M. Hoang, and M. S. Chapman, *Phys. Rev. Lett.* **116**, 155301 (2016).
- [42] L. W. Clark, L. Feng, and C. Chin, *Science* **354**, 606 (2016).
- [43] A. del Campo, *Phys. Rev. Lett.* **121**, 200601 (2018).
- [44] F. J. Gomez-Ruiz, J. J. Mayo, and A. del Campo, *Phys. Rev. Lett.* **124**, 240602 (2020).
- [45] K. Roychowdhury, R. Moessner, and A. Das, *Phys. Rev. B* **104**, 014406 (2021).
- [46] S. Donadello, S. Serafini, T. Bienaimé, F. Dalfovo, G. Lamporesi, and G. Ferrari, *Phys. Rev. A* **94**, 023628 (2016).
- [47] B. Ko, J. W. Park, and Y. Shin, *Nat. Phys.* **15**, 1227 (2019).
- [48] J. Goo, Y. Lim, and Y. Shin, *Phys. Rev. Lett.* **127**, 115701 (2021).
- [49] A. del Campo, G. D. Chiara, G. Morigi, M. B. Plenio, and A. Retzker, *Phys. Rev. Lett.* **105**, 075701 (2010).
- [50] I.-K. Liu, S. Donadello, G. Lamporesi, G. Ferrari, S.-C. Gou, F. Dalfovo, and N. Proukakis, *Commun. Phys.* **1**, 24 (2018).
- [51] M. Chesler, A. M. Garcia-Garcia, and H. Liu, *Phys. Rev. X* **5**, 021015 (2015).
- [52] R. Landig, L. Hruby, N. Dogra, M. Landini, R. Mottl, T. Donner, and T. Esslinger, *Nature* **532**, 476 (2016).
- [53] J. Klinder, H. Keßler, M. R. Bakhtiari, M. Thorwart, and A. Hemmerich, *Phys. Rev. Lett.* **115**, 230403 (2015).
- [54] K. Baumann, C. Guerlin, F. Brennecke, and T. Esslinger, *Nature* **464**, 1301 (2010).
- [55] R. Mottl, F. Brennecke, K. Baumann, R. Landig, T. Donner, and T. Esslinger, *Science* **336**, 1570 (2012).
- [56] H. Wang, S. Li, M. Arzamasovs, W. Liu, and B. Liu, *Phys. Rev. A* **105**, 063301 (2022).
- [57] Y. Chen, Z. Yu, and H. Zhai, *Phys. Rev. A* **93**, 041601(R) (2016).
- [58] N. Dogra, F. Brennecke, S. Huber, and T. Donner, *Phys. Rev. A* **94**, 023632 (2016).
- [59] A. Niederle, G. Morigi, and H. Rieger, *Phys. Rev. A* **94**, 033607 (2016).
- [60] B. Sundar and E. Mueller, *Phys. Rev. A* **94**, 033631 (2016).
- [61] T. Flottat, L. de Forges de Parny, F. Hebert, V. Rousseau, and G. Batrouni, *Phys. Rev. B* **95**, 144501 (2017).
- [62] L. Himbert, C. Cormick, R. Kraus, S. Sharma, and G. Morigi, *Phys. Rev. A* **99**, 043633 (2019).
- [63] E. Burovski, J. Machta, N. Prokof'ev, and B. Svistunov, *Phys. Rev. B* **74**, 132502 (2006).